CHALMERS
UNIVERSITY OF TECHNOLOGY

Channel models for optical transmission systems with polarization dependent losses (PDL)

Master’s thesis in Master Information and Communication Technology

Minoshma Meena

DEPARTMENT OF MICROTECHNOLOGY AND NANOSCIENCE
CHALMERS UNIVERSITY OF TECHNOLOGY
Gothenburg, Sweden 2025
www.chalmers.se

Master's thesis 2025

Channel models for optical transmission systems with polarization dependent losses (PDL)

Minoshma Meena

Department of Microtechnology and Nano Science
Chalmers University of Technology
Gothenburg, Sweden 2025

Channel models for optical transmission systems with polarization dependent losses (PDL)
Minoshma Meena

Supervisor: Magnus Karlsson
Examiner: Magnus Karlsson, Department of Microtechnology and Nano Science

Master's Thesis 2025
Department of Microtechnology and Nano Science
Chalmers University of Technology
SE-412 96 Gothenburg
Telephone +46 31 772 1000

Cover:

Typeset in LaTeX
Printed by Chalmers Reproservice
Gothenburg, Sweden 2025

Channel models for optical transmission systems with polarization dependent losses (PDL)
Minoshma Meena
Department of Microtechnology and Nanoscience
Chalmers University of Technology

Abstract

Polarization Dependent Loss (PDL) presents a important transmission impairment in coherent optical communication systems, originating from components such as wavelength selective switches and reconfigurable optical add-drop multiplexers. This thesis develops advanced channel models to characterize the accumulation of PDL across multi-span optical systems, addressing signal propagation, noise interactions, and capacity constraints. Utilizing Jones matrix formulations and singular value decomposition, the study models individual PDL elements and extends the approach to multi-span configurations through recursive signal evolution, incorporating additive white Gaussian noise (AWGN) from amplifiers.

Statistical analysis reveals sub-linear PDL growth following Maxwellian distributions, confirmed via Monte Carlo simulations. Noise properties exhibit PDL-induced anisotropy in covariance matrices, quantified by eigenvalue ratios, underscoring performance degradation in long-haul networks. Capacity limits for Gaussian signals indicate losses in high-PDL scenarios.

An adapted capacity-achieving scheme, inspired by recent advancements, employs a universal precoder with Linear Minimum Mean Square Error Successive Interference Cancellation (LMMSE-SIC) to transform channels into scalar AWGN subchannels, reducing signal-to-noise ratio (SNR) penalties. Simulations demonstrate enhanced performance compared to standard multiple-input multiple-output (MIMO) approaches, with notable reductions in outage losses.

These methodologies provide insights for enhanced system design for reliable long-haul communication. Future investigations could explore nonlinear effects and insertion loss variations, to enable more competitive optical networks in the future.

Acknowledgements

First and foremost, I would like to express my heartfelt gratitude to **Professor Magnus Karlsson** for welcoming me into the Photonics section and for guiding me patiently throughout my entire master's journey. His readiness to listen and provide clear direction whenever I sought clarification has been invaluable from the very beginning to the completion of this thesis.

I am grateful to **Vijay Shekhawat** and **Ruwan Udayanga** for their practical help whenever it was needed—whether it was arranging prints, assisting with plagiarism checks, or simply making day-to-day tasks easier. Their support has been a quiet but significant part of this work.

I am deeply thankful to **Geo Philip Muppathiyil** , my senior, for being an exceptional mentor and constant source of encouragement. His insights, practical advice, and willingness to share knowledge generously have greatly shaped my understanding and approach to research. To all my friends in Gothenburg: thank you for turning Sweden into a true home for me. Your companionship and warmth have filled this chapter of my life with happiness and belonging.

I also wish to acknowledge **all my former teachers**, whose encouragement over the years inspired me to keep learning and growing. A special thanks goes to **Lena Sommarström**, my study advisor, whose steady motivation and timely guidance always lifted my spirits when challenges arose.

Finally, my deepest love and gratitude go to **my mother and father**. Their unwavering belief in me and endless support have been the foundation of everything I have achieved.

I would also like to acknowledge the assistance of AI tools such as Grok and Grammarly, which helped refine sentence framing and improve the clarity of my writing throughout this thesis.

Minoshma Meena, Gothenburg, Aug 2025

List of Acronyms

Below is the list of acronyms that have been used throughout this thesis listed in alphabetical order:

ASE	Amplified Spontaneous Emission
AWGN	Additive White Gaussian Noise
BER	Bit Error Rate
CN	Circularly Symmetric Complex Gaussian
DWDM	Dense Wavelength Division Multiplexing
EDFA	Erbium-Doped Fiber Amplifier
EIG	Eigenvalue Decomposition
LMMSE	Linear Minimum Mean Square Error
MIMO	Multiple-Input Multiple-Output
PDL	Polarization Dependent Loss
QAM	Quadrature Amplitude Modulation
QPSK	Quadrature Phase Shift Keying
ROADM	Reconfigurable Optical Add-Drop Multiplexer
SIC	Successive Interference Cancellation
SNR	Signal-to-Noise Ratio
SOP	State-of-Polarization
SU(2)	Special Unitary Group of Degree 2
SVD	Singular Value Decomposition
WSS	Wavelength Selective Switch
ROADM	Reconfigurable Optical Add-Drop Multiplexer

Nomenclature

Below is the nomenclature of indices, sets, parameters, variables, operators, and matrices used throughout this thesis.

Indices

i, k	Indices for fiber spans or noise terms in a multi-span optical system
j	Index for matrix products over spans in a multi-span system
N	Total number of spans in the optical system

Sets

$\mathbb{C}^2$	Set of 2-dimensional complex vectors, representing dual-polarization fields

Parameters

A	Per-span polarization-dependent loss (PDL) in decibels
γ	Gain imbalance parameter, quantifying differential attenuation between principal axes
σ_z^2	Total noise variance, scaled for consistent signal-to-noise ratio (SNR) across spans
ρ	Signal-to-noise ratio (SNR), defined as P_x/P_z
Δ	Differential amplification induced by PDL in the noise covariance matrix
θ	Rotation angle for state-of-polarization transformations

α	Normalization factor for unitary matrix construction; also used in PDL severity for capacity-achieving schemes
p_{out}	Outage probability for capacity loss analysis

Variables

$\mathbf{X}$	Optical field vector in a dual-polarization system, representing orthogonal polarization amplitudes
$\mathbf{Y}$	Received signal vector, incorporating noise effects
$\mathbf{Z}_i$	Additive white Gaussian noise (AWGN) for the i-th span, modeled as $\mathcal{CN}(\mathbf{0}, \sigma_z^2 \mathbf{I}_2/N)$
$\mathbf{Z}_{\text{total}}$	Total accumulated noise across all spans
$\mathbf{n}$	Rotation axis vector on the Poincaré sphere
a, b	Complex numbers used to construct unitary matrices for rotations
$\lambda_{\max}, \lambda_{\min}$	Maximum and minimum eigenvalues of the noise covariance matrix, representing principal noise gains
σ_1, σ_2	Singular values from singular value decomposition for PDL computation
e_1, e_2	Eigenvalues used for eigenvalue-based PDL computation
z	Accumulated PDL contribution parameter, proportional to span count
Λ	Effective polarization-dependent loss in decibels
$\langle \Lambda^2 \rangle$	Mean-square PDL, capturing the second moment of the PDL distribution
P_x	Signal power of the input field vector
P_z	Total noise power, derived as $(\mathbf{K})$
C	Achievable channel capacity (bits/s/Hz)
$I(\mathbf{X}; \mathbf{Y})$	Mutual information between input $\mathbf{X}$ and output $\mathbf{Y}$
SNR_i	Per-dimension signal-to-noise ratio for capacity-achieving schemes

Operators and Matrices

$\mathbf{H}_j$	Jones matrix for the j-th fiber span

$\mathbf{H}_{\text{total}}$	Total transfer matrix for a multi-span optical system, defined as $\prod_{j=1}^{N} \mathbf{H}_j$
$\mathbf{U}, \mathbf{V}$	Unitary matrices representing state-of-polarization (SOP) rotations
$\mathbf{D}_\gamma$	Diagonal matrix modeling differential attenuation in a PDL element
$\mathbf{V}^\dagger$	Hermitian conjugate of matrix $\mathbf{V}$, aligning input state-of-polarization
$\mathbf{K}$	Conditional noise covariance matrix, $\mathbb{E}[\mathbf{Z}_{\text{total}}\mathbf{Z}_{\text{total}}^\dagger \mid \{\mathbf{H}_j\}]$
$\mathbf{K}_{\text{before}}$	Noise covariance matrix without PDL, isotropic case
$\mathbf{K}_{\text{after}}$	Noise covariance matrix with PDL, anisotropic case
$\mathbf{P}_i$	Product of channel matrices from span $i+1$ to N, defined as $\prod_{j=i+1}^{N} \mathbf{H}_j$
$\boldsymbol{\sigma}$	Pauli matrices, used for state-of-polarization rotations
$\mathbf{I}_2$	2×2 identity matrix
$\mathbf{W}$	Whitening matrix for capacity-achieving schemes, defined as $\mathbf{U}_D \mathbf{\Sigma}^{-1/2} \mathbf{U}_D^\dagger$
$\mathbf{\Sigma}$	Diagonal matrix of eigenvalues of the noise covariance matrix $\mathbf{K}$
$\mathbf{U}_D$	Eigenvector matrix of the noise covariance matrix $\mathbf{K}$
$\mathbf{H}_{\text{eff}}$	Effective whitened channel matrix, defined as $\mathbf{W}\mathbf{H}_{\text{total}}$
$\mathbf{H}_r$	Real-valued representation of the effective channel matrix
$\widehat{\mathbf{H}}$	Block-diagonal extension of $\mathbf{H}_r$ for two-slot space-time coding
$\mathbf{G}$	Universal real-valued 8×8 precoder matrix for capacity-achieving schemes
$\mathbf{E}$	Linear minimum mean square error (LMMSE) filter matrix
$\mathbf{\Gamma}$	Diagonal matrix of desired gains for LMMSE-SIC scheme
$\mathbf{F}$	Interference terms matrix for LMMSE-SIC scheme

Contents

List of Figures

List of Tables

1

Introduction

In the era of exploding data demands, coherent optical communication systems stand as the backbone of global networks, powering everything from cloud computing to real-time video streaming. These systems leverage dual-polarization transmission over dense wavelength-division multiplexing (DWDM) fibers to squeeze terabits per second into thin spectral slices. Yet, as links stretch across continents—spanning thousands of kilometers with dozens of amplifiers and switches, impairments like polarization-dependent loss (PDL) emerges. PDL arises from components, such as wavelength selective switches and ROADMs, where manufacturing quirks cause light in one polarization to attenuate more than the other. To visualize this, Figure 1.1 illustrates the effect: a balanced input signal enters the PDL element with equal power in both polarizations, but the output shows attenuation in one mode, resulting in a power imbalance that disrupts signal orthogonality.

For context, Figure 1.2 contrasts this with polarization-mode dispersion (PMD), depicting how PMD temporally separates pulses between polarizations, a compensable effect that underscores PDL's unique power-specific challenge[1].

Coupled with fiber birefringence, which randomly scrambles polarization states, PDL doesn't just attenuate signals; it interacts with additive white Gaussian noise (AWGN) from amplifiers, creating uneven noise amplification that warps constellations and inflates bit error rates.

Conventional approaches in the literature typically analyze PDL as a localized effect in individual components or dismiss it for short-reach links, neglecting its cumulative stochastic nature in extended systems. This simplification produces overly optimistic performance estimates, rendering networks susceptible to outages under practical environmental variations. The thesis addresses this limitation by proposing a cohesive framework for PDL in multi-span channels, integrating Jones matrix-based propagation with noise covariance analysis to quantify impairment evolution and capacity degradation. Beginning with -principles modeling of single PDL elements through singular value decomposition, the framework extends to cascaded spans, demonstrating sub-linear accumulation. Here, birefringence-induced SOP rotations decorrelate successive losses, constraining overall growth to approximately $A\sqrt{N}$ dB for per-span PDL A and span count N.

A core contribution lies in elucidating PDL's influence on noise dynamics: it converts isotropic AWGN into anisotropic distributions, where covariance matrices elongate from circular to elliptical forms, as confirmed by Monte Carlo simulations involving 10,000 realizations per configuration. At an SNR of 20 dB, elevated PDL (2 dB per span) induces capacity losses, a degradation that conventional MIMO equalization fails to fully mitigate. To counteract this, the analysis evaluates capacity-achieving techniques, such as precoding combined with successive interference cancellation, which decouples polarizations and restores near-ideal rates with an additional SNR overhead of only 0.5 dB.

This investigation is based on some key assumptions: ASE noise is Gaussian and unaffected by nonlinearities, while CD and PMD are fully compensated via digital signal processing, thereby isolating PDL as the predominant linear impairment.

The thesis proceeds across five chapters. Chapter 2 establishes the Jones matrix foundation for single- and multi-span PDL, deriving Maxwellian statistical distributions. Chapter 3 examines noise anisotropy, measuring distortions through eigenvalue ratios. Chapter 4 derives capacity bounds.

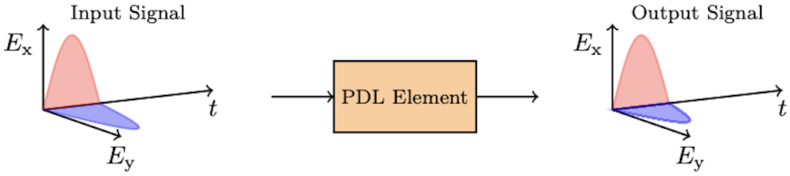

Figure 1.1: Illustration of PDL's power imbalance: balanced input emerges attenuated in one polarization mode.[1]

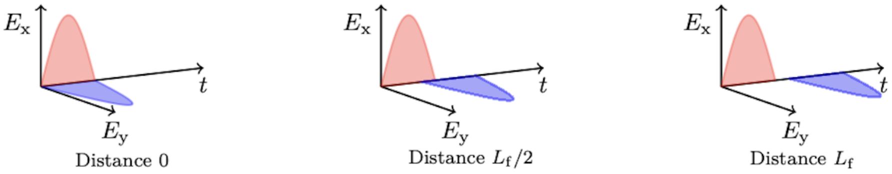

Figure 1.2: Depiction of PMD's temporal pulse separation between x- and y-polarizations.[1]

2

Advanced Channel Modeling of PDL Build-Up in Optical Systems

This chapter provides a description of concatenated Polarization Dependent Loss (PDL) in optical systems, offering a simple Jones matrix model to track signal changes, multi-span signal propagation with noise interactions, and statistical properties such as mean PDL accumulation and Maxwellian distributions to facilitate precise impairment analysis and mitigation in long-haul networks.

Polarization Dependent Loss (PDL) impairs coherent optical communication systems through components, such as wavelength selective switches (WSSs),inline amplifiers and reconfigurable optical add-drop multiplexers (ROADMs)[2] which introduce polarization-dependent signal attenuation. In optical fibers, random polarization rotations, driven by birefringence and environmental perturbations, induce stochastic variations in the signal's polarization state, which, in multi-span coherent optical systems, couple with PDL to interact with Additive White Gaussian Noise (AWGN), resulting in non-uniform noise amplification and significant time-varying signal degradation across the link. This necessitates advanced channel models for long-haul systems where PDL accumulates. In this context, channel models are mathematical frameworks that characterize signal propagation through multi-span optical links, capturing the cumulative effects of PDL, polarization rotations, and noise interactions to predict system performance. Prior studies often focused on isolated PDL effects in single components or assumed negligible polarization impairments, overlooking the stochastic and cumulative nature of PDL in multi-span systems. Advanced channel models are critical, as they provide a comprehensive framework to analyze PDL-induced impairments across extended networks, enabling precise system design and effective mitigation strategies for reliable long-haul optical communication.

2.1 Modeling a Single PDL Element

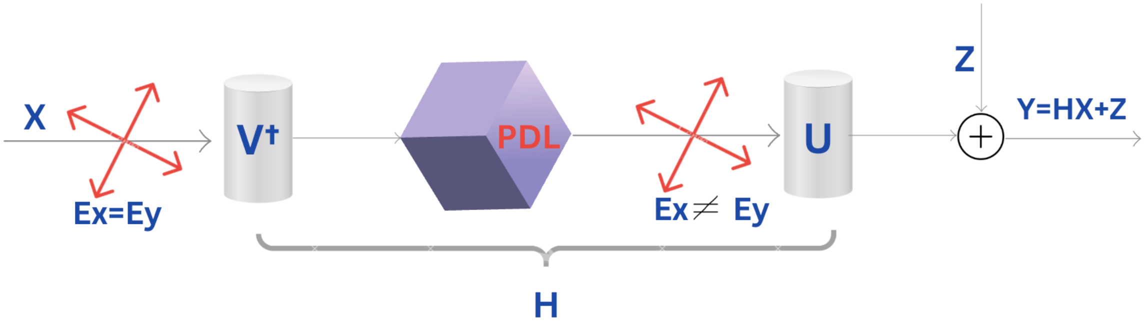

Figure 2.1: 3D block diagram of a single PDL element showing the signal flow from input $X(X_1, X_2)$ through the PDL element.

2.1.1 Jones Matrix Formulation

The optical amplitude in a dual-polarization system is represented as a 2D complex vector:

$$X = \begin{pmatrix} X_1 \\ X_2 \end{pmatrix} \in \mathbb{C}^2, \tag{2.1}$$

where X_1 and X_2 denote the orthogonal polarization amplitudes. A PDL element's effect is modeled using a 2×2 Jones matrix, expressed via Singular Value Decomposition (SVD):

$$H = U D_\gamma V^\dagger, \tag{2.2}$$

where $U, V \in SU(2)$ are two unitary matrices responsible for lossless State-of-Polarization (SOP) rotations, The matrix $V^\dagger$ rotates the input SOP to align with the principal axes of the PDL element, D_γ applies the differential attenuation, and U subsequently rotates the SOP post-attenuation, capturing the birefringence-induced transformations in the optical system. The diagonal matrix

$$D_\gamma = \begin{pmatrix} \sqrt{1+\gamma} & 0 \\ 0 & \sqrt{1-\gamma} \end{pmatrix}, \quad \gamma \in [0, 1], \tag{2.3}$$

represents the gain imbalance, with the ratio of maximum to minimum power gains given by $\frac{P_{\max}}{P_{\min}} = \frac{1+\gamma}{1-\gamma}$, where γ quantifies the differential attenuation (anisotropic loss) between the principal axes of the PDL element. Special cases include: $\gamma = 0$, where $D_\gamma = I$ (the identity matrix), indicating no gain imbalance and equal power along both principal axes due to the absence of PDL; and $\gamma = 1$, where D_γ becomes $\begin{pmatrix} \sqrt{2} & 0 \\ 0 & 0 \end{pmatrix}$, representing complete attenuation along one axis and maximum imbalance, justified by the physical limit of total polarization-dependent loss.

2.1.2 Modeling Birefringence and SOP Rotations

Fiber birefringence induces SOP rotations, which can be visualized as rotations on the Poincaré sphere. These rotations are mathematically described by unitary matrices ($U, V \in SU(2)$), where any $SU(2)$ matrix can be expressed as:

$$U = \exp\left(i\frac{\theta}{2}\mathbf{n}\cdot\boldsymbol{\sigma}\right), \tag{2.4}$$

with $\boldsymbol{\sigma}$ representing the Pauli matrices [3] and $\mathbf{n}$ denoting the rotation axis on the Poincaré sphere. The parameter θ determines the angle of rotation.

To simulate random SOP rotations, the unitary matrices U and V are generated using complex numbers $a = a_{\text{real}} + ia_{\text{imag}}$ and $b = b_{\text{real}} + ib_{\text{imag}}$, where $a_{\text{real}}, a_{\text{imag}}, b_{\text{real}}, b_{\text{imag}} \sim \mathcal{N}(0,1)$. A normalization factor is computed as $\alpha = \sqrt{|a|^2 + |b|^2}$, and the matrix is constructed as:

$$U = \frac{1}{\alpha}\begin{pmatrix} a & b \\ -\overline{b} & \overline{a} \end{pmatrix}, \tag{2.5}$$

where $\overline{a}, \overline{b}$ are the complex conjugates, ensuring $U^\dagger U = I$. This construction parametrisizes the special unitary group $SU(2)$ according to the Haar measure[4], providing statistical validity for simulating random SOP rotations. These rotations are essential for modeling sub-linear PDL accumulation in multi-span optical systems, a key focus of this thesis.

2.1.3 PDL-Free Fiber and Unitary Transformations

In a lossless fiber ($\gamma = 0$), the differential attenuation matrix simplifies to $D_\gamma = I$, the identity matrix. Consequently, the Jones matrix becomes:

$$H = UV^\dagger, \tag{2.6}$$

which is unitary, as

$$H^\dagger H = (VU^\dagger)(UV^\dagger) = I. \tag{2.7}$$

This unitarity guarantees conservation of optical power, as the SOP undergoes pure rotations without attenuation.

2.1.4 Output with Noise

The received signal, incorporating noise, is usually modeled as:(fig:2.1)

$$Y = HX + Z, \quad Z \sim \mathcal{CN}(0, I_2), \tag{2.8}$$

where Z represents Additive White Gaussian Noise (AWGN) introduced by Erbium-Doped Fiber Amplifiers (EDFAs). The output power is given by:

$$Y^\dagger Y = X^\dagger H^\dagger H X. \tag{2.9}$$

Here, $H^\dagger H = VD_\gamma^2V^\dagger$. The SVD decomposition uniquely separates the SOP rotations (U, V) and the loss (D_γ). The parameter γ typically corresponds to differential losses of 0.3–0.6 dB for commercial Wavelength Selective Switches (WSSs)[5], for example, the Santec WSS-100 reports a maximum PDL of 0.53 dB and average 0.27 dB [6][7].

2.2 Multi-Span Channel Model

The optical channel under investigation is characterized by a multi-span configuration, comprising N consecutive fiber spans, each contributing to the cumulative polarization-dependent loss (PDL) and state-of-polarization (SOP) transformations. In this concatenated setup (see Figure 2.2), the input light X enters the first span, where it undergoes SOP "spin" rotations via U_1 and $V_1^\dagger$, followed by differential attenuation from PDL in D_{γ_1}, yielding an output that propagates into the fiber. This output is then perturbed by AWGN Z_1 from the amplifier, influencing the signal entering the next span. Subsequent spans repeat this cycle—rotations, PDL effects, and noise addition—cascading impairments where prior noise Z_i is further transformed by downstream, amplifying non-uniform degradation across polarizations. The total transfer matrix, denoted H_{total}, is defined as the ordered product of individual span matrices:

$$H_{\text{total}} = \prod_{i=N}^{1} H_i, \tag{2.10}$$

where H_i represents the Jones matrix for the i-th span. This formulation serves as a pivotal element of the thesis, providing a comprehensive framework to elucidate the aggregated impact of PDL across extended optical networks. The received signal Y evolves through a series of transformations that encapsulate the sequential propagation dynamics across multiple spans, a process critical to the design and optimization of resilient long-haul communication systems.

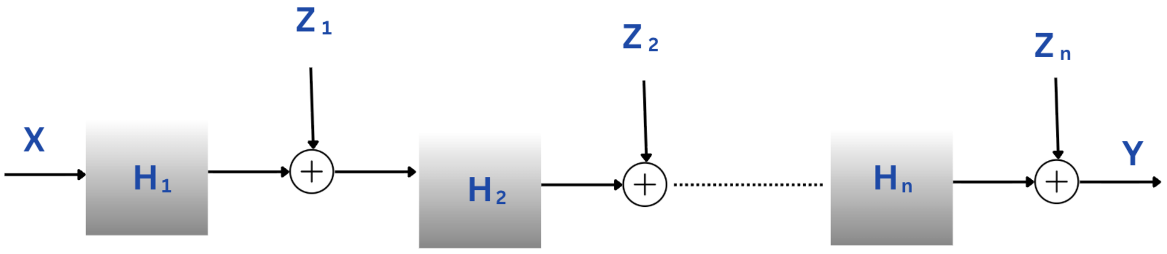

Figure 2.2: n-span channel configuration illustrating distributed PDL elements.

The signal evolution can be expressed recursively, reflecting the incremental contributions of each span through a sequential processing formulation[8]:

- For $N = 1$: $Y = H_1X + Z_1$,
- For $N = 2$: $Y = (H_1X + Z_1)H_2 + Z_2 = H_2H_1X + H_2Z_1 + Z_2$,
- For $N = 3$: $Y = [(H_1X+Z_1)H_2+Z_2]H_3+Z_3 = H_3H_2H_1X+H_3H_2Z_1+H_3Z_2+Z_3$,

Generalizing to an arbitrary number of spans N, the received signal is given by:

$$Y = H_{\text{total}}X + \sum_{i=1}^{N} \left(\prod_{j=i+1}^{N} H_j \right) Z_i, \quad Z_i \sim \mathcal{CN}(0, I_2), \tag{2.11}$$

where Z_i denotes the additive white Gaussian noise (AWGN) introduced by the amplifier in the i-th span, modeled as a complex circularly symmetric Gaussian random variable with zero mean and identity covariance matrix I_2.

This recursive formulation represents a significant advancement, capturing the compounded effect of PDL and the progressive accumulation of ASE noise across the link. The proposed model distinguishes itself through its dual-component structure:

(i) The deterministic term $H_{\text{total}}X$, which encodes the concatenated PDL and SOP rotations induced by birefringence across all spans

(ii) The stochastic term $\sum_{i=1}^{N} \left(\prod_{j=i+1}^{N} H_j \right) Z_i$, which quantifies the cascading noise contributions.

As a result, a network with distributed PDL elements, termed a PDL channel, emulates a single PDL component, where an effective Λ integrates the PDL contributions from the individual impaired segments, alongside a correlated noise Z. According to Equation (2.11), the presence of multiple transfer matrices in this distributed setup can be reduced to the analysis of a simplified channel model, which is elaborated in the following section.

2.3 Characterization of Channel Statistics

2.3.1 PDL Statistical Analysis

The effective polarization-dependent loss (PDL) is determined by the real eigenvalues $\lambda_{\max}$ and $\lambda_{\min}$ of the Hermitian matrix $H_{\text{total}}^{\dagger}H_{\text{total}}$, computed across N spans as per the multi-span channel model. The PDL is expressed as:

$$\Lambda = 10\log_{10}\left(\frac{\lambda_{\max}}{\lambda_{\min}}\right), \tag{2.12}$$

where $\lambda_{\max}$ and $\lambda_{\min}$ represent the maximum and minimum gains along the principal polarization states, respectively, serving as a metric for gain imbalance. This definition ties directly to the gain imbalance parameter γ, defined by[8]:

$$\gamma = \frac{10^{A/10} - 1}{10^{A/10} + 1}, \tag{2.13}$$

where A denotes the per-span PDL in decibels (dB), reflecting the intrinsic polarization-dependent loss introduced by each optical element within a span, typically ranging from 0.1 to 2 dB in practical systems. For the energy-conserving model, the PDL can also be expressed in terms of γ as:

$$\Lambda = 10\log_{10}\left(\frac{\sqrt{1+\gamma}}{\sqrt{1-\gamma}}\right) \tag{2.14}$$

A comprehensive simulation study was conducted to characterize the PDL distribution. The analysis spanned per-span PDL values $A = \{0.2, 0.6, 1.0, 1.2\}$ dB, with the number of spans N ranging from 1 to 25, where H_i represents the Jones matrix for the i-th span. The mean PDL is calculated via Monte Carlo simulation: For fixed per-span PDL A (dB) and spans N, generates total Jones matrix $H_{\text{total}} = \prod_{i=N}^{1} H_i$, where each $H_i = U_i D_\gamma V_i^\dagger$ (random Haar unitaries U_i, V_i; fixed D_γ from $\gamma = \frac{10^{A/10}-1}{10^{A/10}+1}$). For each realization, compute total PDL as $\Lambda = 10\log_{10}(\lambda_{\max}/\lambda_{\min})$ from eigenvalues of Hermitian $H_{\text{total}}^\dagger H_{\text{total}}$. The mean is the arithmetic average over these Λ values: $\langle\Lambda\rangle = \frac{1}{10{,}000}\sum \Lambda^{(r)}$. This formulation serves as an important element of the thesis, providing a comprehensive understanding of the impact of PDL across extended optical networks(see Table 2.1).

Table 2.1: Mean PDL (dB) for Various A and N Values from 10,000 Realizations

N	$A = 0.2$ dB	$A = 0.6$ dB	$A = 1.0$ dB	$A = 1.2$ dB
1	0.2000	0.6000	1.0000	1.2000
5	0.4173	1.2453	2.0675	2.5120
10	0.5863	1.7609	2.9301	3.5506
15	0.7128	2.1447	3.6251	4.3352
20	0.8333	2.4929	4.2160	5.0712
25	0.9249	2.8195	4.7449	5.7220

The mean PDL exhibits a sub-linear increase with N, a trend driven by the statistical averaging of random SOP rotations, which reduces the cumulative PDL growth. As depicted in Figure 3.2 this behavior can be qualitatively linked to a square root dependence on N modulated by A. However, the random unitary transformations U_i and V_i introduce decorrelation, leading to a mean PDL that scales approximately as $A\sqrt{N}$ for low N, before saturating due to averaging[9]. For instance, with $A = 0.2$ dB, the mean PDL rises from 0.2000 dB at $N = 1$ to 0.9249 dB at $N = 25$, far below a linear extrapolation of $0.2 \times 25 = 5$ dB, supporting the $\sqrt{N}$ influence. This sub-linear growth, noticeable beyond $N = 15$, highlights the complex dynamics of PDL accumulation, offering critical insights for long-haul optical network design.

2.3.1.1 Methodological Validation

The accuracy of PDL estimation was validated by comparing the eigenvalue decomposition (EIG) and singular value decomposition (SVD) methods, which are highly relevant

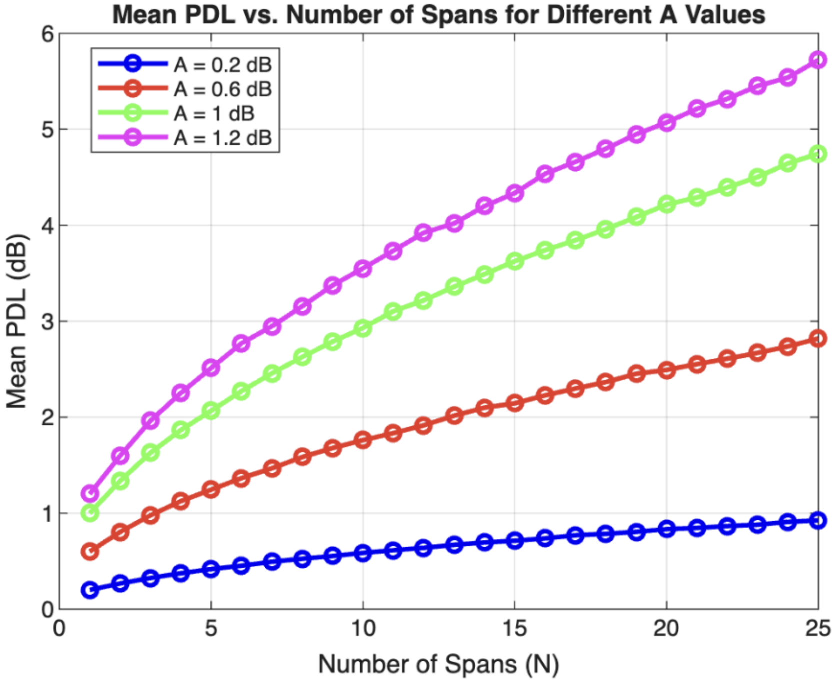

Figure 2.3: Mean PDL vs. number of spans N for per-span PDL values $A = \{0.2, 0.6, 1.0, 1.2\}$ dB.[10]

for analyzing PDL concatenation in multi-span systems. The EIG method, based on the eigenvalues e_1 and e_2 of $H^{\dagger}_{\text{total}} H_{\text{total}}$, computes PDL as:

$$\Lambda_{\text{dB, EIG}} = 10 \cdot \log_{10}\left(\frac{e_1}{e_2}\right), \tag{2.15}$$

while the SVD method, derived from the singular values $\sigma_1 \geq \sigma_2 \geq 0$ of total transfer matrix H_{total}

$$\Lambda_{\text{dB, SVD}} = 10 \cdot \log_{10}\left(\frac{\sigma_1}{\sigma_2}\right)^2 = 20 \cdot \log_{10}\left(\frac{\sigma_1}{\sigma_2}\right), \tag{2.16}$$

with equivalence established via $e_1 = \sigma_1^2$ and $e_2 = \sigma_2^2$. A simulation spanning N from 1 to 100 and A from 0 to 2 dB demonstrated identical mean PDL values, underscoring the overlapping behavior of EIG and SVD. This consistency is vital for PDL concatenation studies, as both methods effectively isolate the gain disparity along principal polarization states, enabling precise tracking of accumulation as N increases.

In real long-haul optical systems, such as transatlantic or transcontinental links spanning 6,000–12,000 km, the number of spans typically ranges from 60 to 240, with an average span length of 50–100 km facilitated by erbium-doped fiber amplifiers (EDFAs), each span contains 1–5 PDL-inducing elements with 1–2 elements per span being prevalent in modern dense wavelength division multiplexing (DWDM) systems. Extending the thesis model to these realistic scenarios is imperative, as the sub-linear PDL accumulation

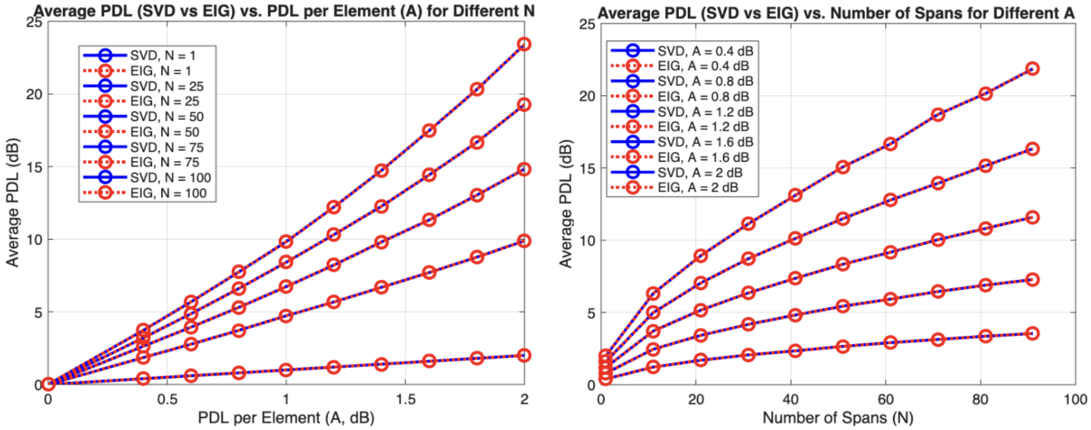

(a) EIG and SVD PDL estimation for $N = 1$ to 100 and $A = 0$ to 2 dB

(b) EIG and SVD PDL estimation for $A = 0$ to 2 dB and $N = 1$ to 100.

Figure 2.4: Validation of PDL estimation methods across varying span counts and PDL levels.

observed (e.g., 0.9249 dB for $A = 0.2$ dB over 25 spans) suggests that PDL impairments may become significant beyond 15–20 spans, potentially reaching 2–5 dB in 80–120 span systems. Addressing PDL impairments is crucial because they degrade signal quality, increase bit error rates, and necessitate advanced compensation techniques, such as polarization tracking or adaptive equalization, to maintain performance in high-capacity DWDM networks, thereby underscoring the practical relevance of this research.

2.3.2 Maxwellian Distribution Analysis

Random state-of-polarization rotations in multi-span optical systems, modeled by Jones matrices with random unitary transformations, produce a Maxwellian PDL distribution in decibels [11, 12]. This arises as the random unitary matrices ensure independent polarization transformations, mimicking a three-dimensional Gaussian random walk in Stokes space, where the PDL magnitude $\Lambda(z)$ follows a chi distribution with three degrees of freedom (equivalent to Maxwellian, as $\Lambda^2(z)$ is chi-squared), due to the correspondence between Jones matrix singular values and Stokes space power gains, enabling efficient numerical simulations of the distribution.

Comparing simulated and theoretical Maxwellian distributions of PDL is essential for validating the stochastic model and assessing system performance limits, as the theoretical framework, rooted in a random walk model of PDL accumulation [11], serves as an ideal benchmark. The distribution is mathematically represented by the probability density function:

$$f(\Lambda; z) = \sqrt{\frac{2}{\pi}} \frac{\Lambda^2}{[\sigma(z)]^3} \exp\left(-\frac{\Lambda^2}{2[\sigma(z)]^2}\right), \tag{2.17}$$

Table 2.2: Mean PDL Values from Simulations for $N = 25$ Spans

A (dB)	Mean PDL (dB)	$A\sqrt{N}$ (dB)
0.4	1.85	2.0
0.6	2.78	3.0
0.8	3.73	4.0
1.0	4.69	5.0
1.6	7.72	8.0
2.4	12.16	12.0

where $\Lambda(z)$ denotes the PDL magnitude in linear units at link position z, $\sigma^2(z)$ is the per-component scale variance quantifying the Gaussian spread in Stokes space (tied to the mean-square PDL), and the prefactor normalizes the distribution while the exponential governs the decay of probability for large Λ, reflecting the chi-squared tail. The scale $\sigma^2(z)$ is defined as:

$$\sigma^2(z) = \frac{\langle \Lambda^2(z) \rangle}{3}, \tag{2.18}$$

where $\langle \Lambda^2(z) \rangle$ is the mean-square PDL (second moment, capturing average squared deviation from unity gain), with the $1/3$ accounting for the three-dimensional random walk. To avoid confusion, note that $\sigma^2(z)$ is *not* the variance of $\Lambda(z)$: $\mathrm{Var}(\Lambda(z)) = \langle \Lambda^2(z) \rangle - \langle \Lambda(z) \rangle^2 = \sigma^2(z)(3 - 8/\pi) \approx 0.4535\sigma^2(z) \approx 0.1512\langle \Lambda^2(z) \rangle$, the reduced spread of the magnitude due to vector summation.

The mean PDL $\langle \Lambda(z) \rangle$ (average differential transmission) is:

$$\langle \Lambda(z) \rangle = \sqrt{\frac{8\sigma^2(z)}{\pi}} = \sqrt{\frac{8\langle \Lambda^2(z) \rangle}{3\pi}} \approx 1.5958\,\sigma(z) \approx 0.9207\sqrt{\langle \Lambda^2(z) \rangle}, \tag{2.19}$$

The mean-square PDL can be further expressed as:

$$\langle \Lambda^2(z) \rangle = \frac{\gamma_1^2}{2}\left(\exp\left(\frac{2z}{\gamma_1^2}\right) - 1\right), \tag{2.20}$$

where $\gamma_1 = 20/\ln(10) \approx 8.686$ is the dB-to-linear conversion factor (from $\Lambda_{\mathrm{dB}} \approx \gamma_1 \Lambda$ for small Λ), and z is the accumulated PDL strength parameter ($z \propto N\times$ mean-square PDL per span).

Simulations with 100,000 realizations incorporate practical effects such as finite sampling and numerical errors, revealing non-linear PDL growth for large per-span PDL due to the breakdown of the small-z approximation—where z becomes significant compared to γ_1^2, invalidating linear approximations—as well as statistical fluctuations and potential SOP decorrelation, underscoring the need for adaptive models in high-PDL scenarios.

As shown in Figure 2.5, the overlaid simulated and theoretical PDL distributions reveal differences in the high-PDL tails.

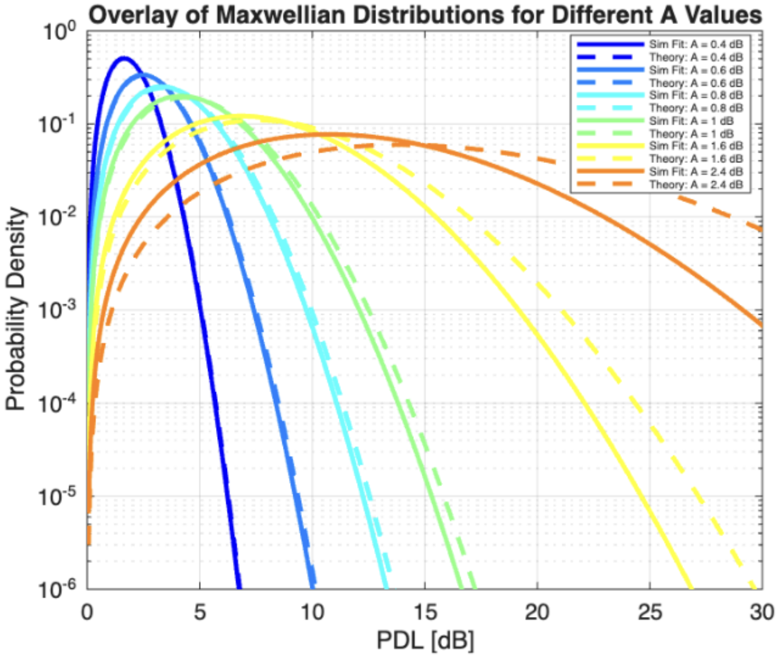

Figure 2.5: Overlay of PDL Distributions - Deviations from Maxwellian Behavior

Figure 2.6 illustrates the PDL distribution's response to increasing per-span PDL (A) from 0.4 to 2.4 dB for 25 spans, showing a transition from sharp, symmetric profiles at low A (e.g., 0.4 dB) to broader, less symmetric shapes with elongated tails at high A (e.g., 2.4 dB), with mean PDL values escalating as per Table 2.2. The overlay in Figure 2.5 integrates these distributions to affirm this evolution, revealing a progressive loss of Maxwellian traits—flattening peaks and extended tails—as mean PDL¢¢ exceeds 12.16 dB, where the simulated mean deviates slightly from the theoretical prediction due to the small-z approximation, which holds for low per-span PDL but fails at high per-span PDL ($A = 2.4\,\mathrm{dB}$), causing non-linear PDL growth amplified by statistical fluctuations and numerical errors, suggesting that the model effectively captures moderate PDL levels.

The figure 2.7 trace the PDL distribution's development as the number of spans (N) increases under a fixed per-span PDL (A). At $N = 6$, the distribution lacks a distinct Maxwellian peak and exhibits misaligned tails, indicating insufficient SOP randomization. With $N = 16$, a clearer peak emerges alongside improved tail alignment, suggesting a step toward Maxwellian traits. At $N = 26$, the peak sharpens and tails conform better, reflecting enhanced stochastic averaging. By $N = 41$, the distribution stabilizes into a Maxwellian-like form, implying that adequate span counts foster robust PDL accumulation. This progression highlights the pivotal role of N in shaping PDL statistics, offering critical guidance for optimizing multi-span optical network designs.

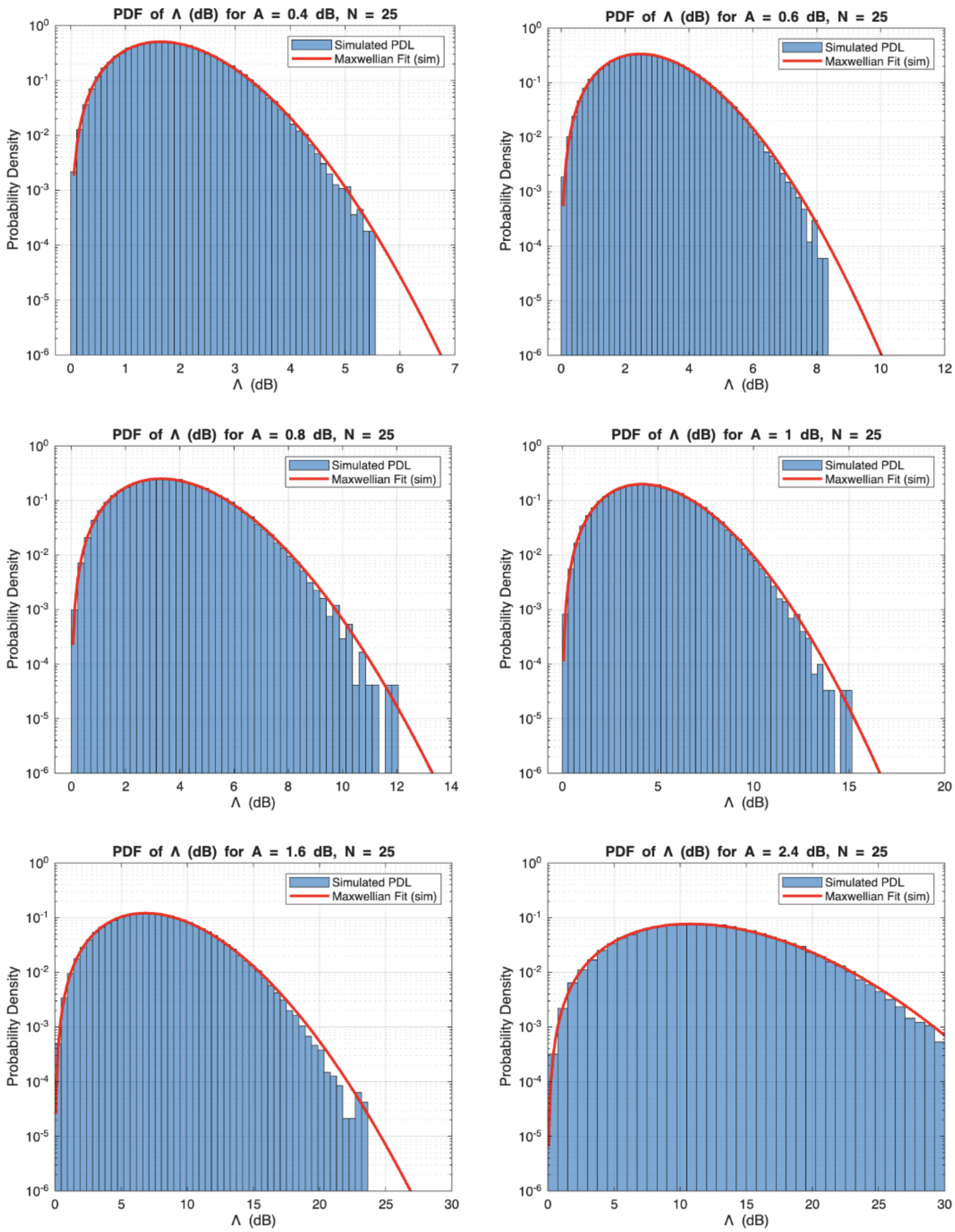

Figure 2.6: PDL Distribution Evolution with Varying Per-Span PDL at Constant Spans ($N = 25$)

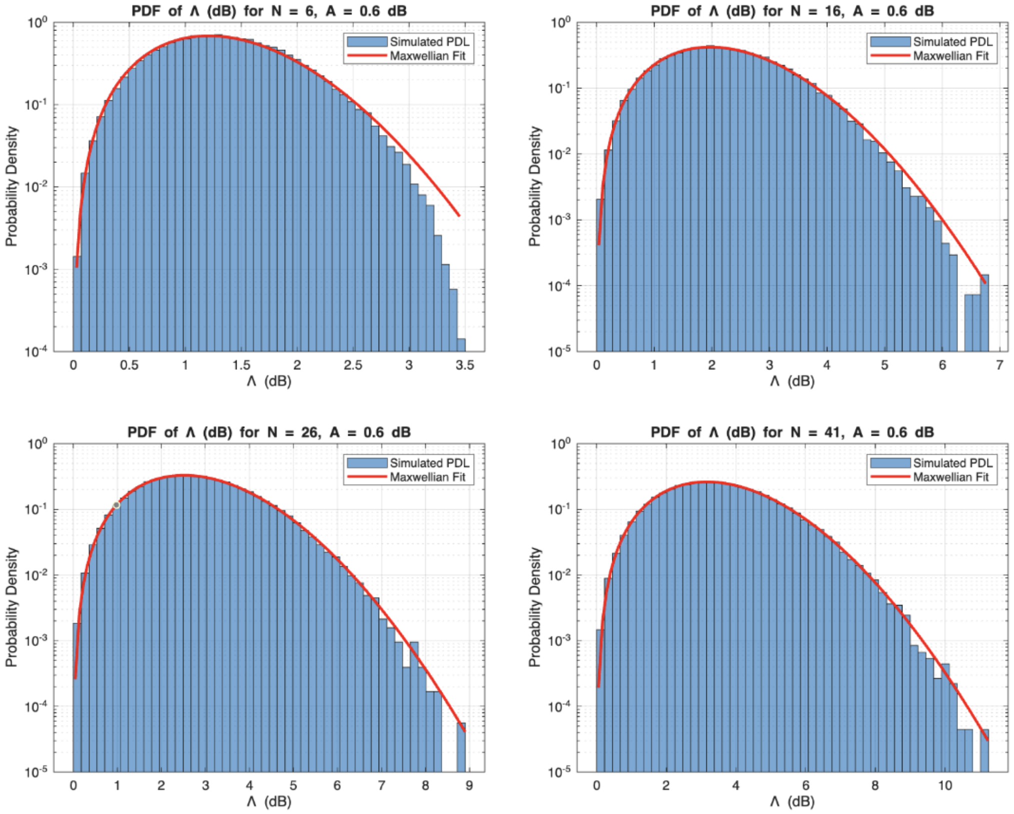

Figure 2.7: PDL Distribution Evolution with Increasing Number of Spans at Fixed Per-Span PDL

3

Noise Characteristics in Multi-Span Links

This chapter delves into the interaction between polarization-dependent loss (PDL) and additive white Gaussian noise (AWGN) in multi-span coherent optical systems, focusing on how PDL alters the noise covariance matrix from isotropic to anisotropic forms. Building upon the PDL accumulation models from previous chapters, using the noise covariance expression, the analysis aims to validates through extensive Monte Carlo simulations quantifying anisotropy via eigenvalue ratios. And discuss system performance impacts with mitigation approaches. This analysis highlights the noise anisotropy and propagation of noise through subsequent spans, offering insights for accurate channel modeling in long-haul networks.

3.1 Modeling the Noise Covariance Matrix

The multi-span channel model, as established in Section 2.2, describes the received field $\mathbf{Y} \in \mathbb{C}^2$ as:

$$\mathbf{Y} = \mathbf{H}_{\text{total}}\mathbf{X} + \mathbf{Z}_{\text{total}}, \tag{3.1}$$

where $\mathbf{H}_{\text{total}} = \prod_{j=1}^{N} \mathbf{H}_j$, $\mathbf{X} \in \mathbb{C}^2$ is the input dual-polarization field, and $\mathbf{Z}_{\text{total}}$ aggregates the noise:

$$\mathbf{Z}_{\text{total}} = \sum_{i=1}^{N} \left(\prod_{j=i+1}^{N} \mathbf{H}_j \right) \mathbf{Z}_i. \tag{3.2}$$

Here, $\mathbf{Z}_i \sim \mathcal{CN}(\mathbf{0}, \sigma_z^2 \mathbf{I}_2/N)$ models the circularly symmetric complex Gaussian noise from the i-th amplifier, scaled to yield a fixed total variance σ_z^2 independent of N for fair SNR comparisons.

The conditional covariance $\mathbf{K} = \mathbb{E}[\mathbf{Z}_{\text{total}}\mathbf{Z}_{\text{total}}^\dagger \mid \{\mathbf{H}_j\}]$, given a specific PDL configuration, is obtained by expressing the outer product[13]:

$$\mathbf{Z}_{\text{total}}\mathbf{Z}_{\text{total}}^\dagger = \left(\sum_{i=1}^{N} \left(\prod_{j=i+1}^{N} \mathbf{H}_j \right) \mathbf{Z}_i \right) \left(\sum_{k=1}^{N} \mathbf{Z}_k^\dagger \left(\prod_{j=k+1}^{N} \mathbf{H}_j \right)^\dagger \right) \tag{3.3}$$

Averaging over the noise (each $\mathbf{Z}_i$ being proper Gaussian with $\mathbb{E}[\mathbf{Z}_i\mathbf{Z}_k^T] = \mathbf{0}\delta_{ik}$):

$$\mathbb{E}[\mathbf{Z}_{\text{total}}\mathbf{Z}_{\text{total}}^{\dagger}] = \sum_{i=1}^{N}\sum_{k=1}^{N}\left(\prod_{j=i+1}^{N}\mathbf{H}_j\right)\mathbb{E}[\mathbf{Z}_i\mathbf{Z}_k^{\dagger}]\left(\prod_{j=k+1}^{N}\mathbf{H}_j\right)^{\dagger}, \quad (3.4)$$

where linearity permits interchanging the sum and expectation. Given the independence and zero-mean nature of the $\mathbf{Z}_i$[7]:

$$\mathbb{E}[\mathbf{Z}_i\mathbf{Z}_k^{\dagger}] = \delta_{ik}\cdot\frac{\sigma_z^2}{N}\mathbf{I}_2, \quad (3.5)$$

off-diagonal terms ($i \neq k$) disappear, resulting in:

$$\mathbf{K} = \frac{\sigma_z^2}{N}\sum_{i=1}^{N}\left(\prod_{j=i+1}^{N}\mathbf{H}_j\right)\left(\prod_{j=i+1}^{N}\mathbf{H}_j\right)^{\dagger} = \frac{\sigma_z^2}{N}\sum_{i=1}^{N}\mathbf{P}_i\mathbf{P}_i^{\dagger}, \quad (3.6)$$

with $\mathbf{P}_i = \prod_{j=i+1}^{N}\mathbf{H}_j$. This form, a Hermitian and positive-definite operator, illustrates how PDL differentially amplifies noise components.

Without PDL, the unitarity of $\mathbf{H}_j$ implies $\mathbf{P}_i\mathbf{P}_i^{\dagger} = \mathbf{I}_2$, hence $\mathbf{K} = \sigma_z^2\mathbf{I}_2$, maintaining equal variance across polarizations without correlations. The expected covariance matrix before PDL, in this isotropic case, is thus:

$$\mathbf{K}_{\text{before}} = \begin{pmatrix}\sigma_z^2 & 0\\ 0 & \sigma_z^2\end{pmatrix},$$

where the diagonal elements are equal, reflecting uniform noise power across the two polarization modes due to the absence of differential amplification. This is justified by the unitarity of $\mathbf{H}_j$, which preserves the norm of the noise vector, ensuring no correlation or variance imbalance.

In the presence of PDL, the diagonal PDL matrix (with unequal eigenvalues from the high and low gain axes) creates noise anisotropy: noise power ends up different between the two polarization modes because of random SOP rotations along the link. The covariance matrix $\mathbf{K}$ from Eq. 3.6 takes a general 2x2 Hermitian shape:

$$\mathbf{K} = \begin{pmatrix}k_{11} & k_{12}\\ k_{12}^{*} & k_{22}\end{pmatrix},$$

where the diagonals k_{11} and k_{22} show the variances in each mode (one boosted, one suppressed by PDL), the off-diagonal $|k_{12}|$ captures mixing from rotations, and the total trace $k_{11} + k_{22} \geq 2\sigma_z^2$ reflects extra noise power from amplified early contributions. This setup is exact—PDL's non-unitary scaling (gains not equal to 1) differentially boosts noise as it travels. Measured anisotropy with the eigenvalue ratio $\lambda_{\max}/\lambda_{\min}$ of $\mathbf{K}$: close to 1 means nearly even noise (isotropic), while bigger numbers (>2) mean strong polarization imbalance, as seen in upcoming simulation results.

3.1.1 Numerical Validation and Simulation Results

To validate the derived noise covariance model and quantify the PDL-induced anisotropy, extensive Monte Carlo simulations were conducted, building on the Jones matrix framework from Section 2.1 and the multi-span model from Section 2.2. The simulation setup mirrors practical long-haul systems with $N = 25$ spans, each containing one PDL element, and per-span PDL values $A \in \{0, 0.2, 0.6, 1.0, 1.5, 2.0, 2.2, 2.4\}$ dB. Noise samples $\mathbf{Z}_i$ were drawn from $\mathcal{CN}(\mathbf{0}, \sigma_z^2 \mathbf{I}_2/N)$ with $\sigma_z = 0.3$, normalized for consistent total variance across spans. For each realization (10,000 total per A), the total noise $\mathbf{Z}_{\text{total}}$ was computed both with PDL (after) and without (before) to isolate PDL effects. The covariance matrices were estimated empirically, and their eigenvalues were used to compute the anisotropy ratio $\lambda_{\text{max}_n}/\lambda_{\text{min}_n}$.

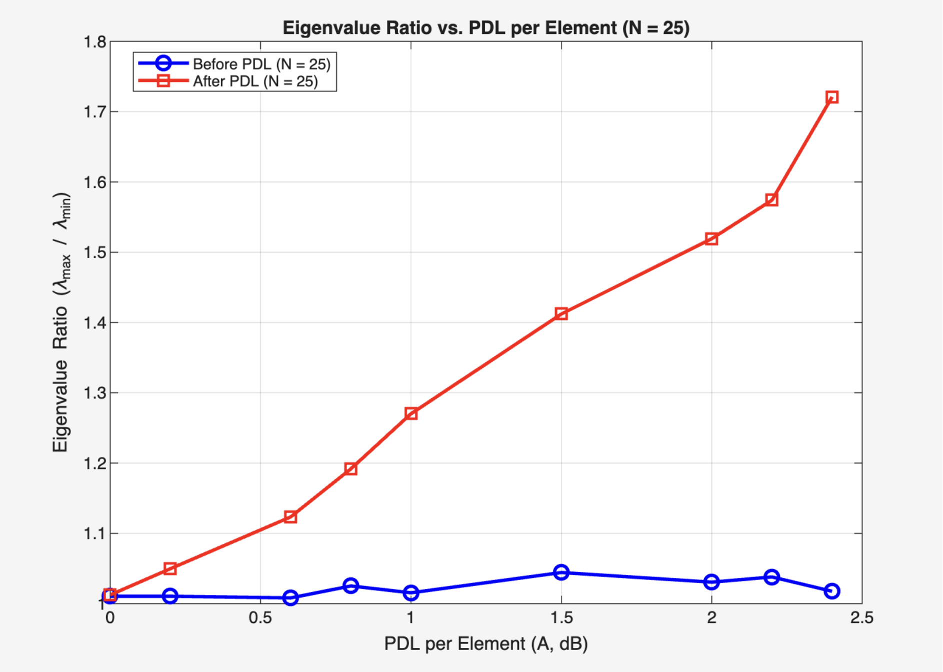

Figure 3.1: Eigenvalue Ratio vs. Per-Span PDL A for $N = 25$, Showing Transition from Isotropy to Anisotropy with a Notable Change at $A \approx 0.6$ dB

Table 3.1 summarizes the key metrics, including mean PDL (consistent with Section 2.3) and eigenvalue ratios. The random number generator was seeded for reproducibility, and minor variations in "before PDL" ratios (around 1.0246 on average) are attributable to finite sampling, confirming near-isotropy in the absence of PDL.

The results validate the model: before PDL, ratios remain close to 1 across all A values, confirming the expected isotropy of the noise distribution. After PDL, ratios exhibit a nonlinear increase with A, indicating growing anisotropy driven by cumulative differential amplification across spans. For low A (e.g., 0.2 dB), the ratio is moderate (1.1709), supporting the adequacy of the standard AWGN model; for high A (e.g., 2.4

Table 3.1: Mean PDL and Noise Covariance Eigenvalue Ratios for $N = 25$ Spans (10,000 Realizations)

A (dB)	Mean PDL (dB)	Eig. Ratio No PDL	Eig. ratio with PDL
0.0	0.0000	1.0246	1.0246
0.2	0.9231	1.0249	1.1709
0.6	2.7966	1.0374	1.2934
1.0	4.6855	1.0240	1.4145
1.5	7.1630	1.0047	2.2367
2.0	9.8496	1.0034	2.3346
2.2	10.9488	1.0430	3.8765
2.4	12.1355	1.0236	4.2007

dB), it rises to 4.2007, highlighting the need for an adapted model to ensure precise performance prediction in DWDM network systems.

To visualize the combined results, Figure 3.1 presents a comprehensive overview, beginning with the eigenvalue ratio plot followed by Figure 3.2 of $\Re(Z_1)$ vs. $\Re(Z_2)$ for all tested A values (before and after PDL) arranged in a grid. The eigenvalue ratio plot illustrates the transition from isotropy to anisotropy, with a significant change becoming evident at $A \approx 0.6$ dB, where the ratio begins to deviate notably from 1. The scatter plots use 10,000 subsampled realizations overlaid with 95% confidence ellipses derived from eigenvalue decomposition of the empirical covariance , where the major and minor axes of the ellipses reflect the polarization-dependent noise variance, with the major axis aligning with the dominant polarization mode and the minor axis indicating the suppressed mode due to PDL. This integrated figure highlights the progression from isotropy at low A to pronounced anisotropy at higher A, corroborating the simulation data and model predictions.

3.1.2 Impact on System Performance and Mitigation Strategies

The quantified noise anisotropy has direct implications for system performance in coherent optical networks. For instance, elevated eigenvalue ratios degrade the effective signal-to-noise ratio (SNR) by unevenly amplifying noise in one polarization mode, potentially increasing bit error rates (BER) in modulation formats like QPSK or 16-QAM [14]. In high-PDL regimes ($A > 1.5$ dB), the adapted bivariate AWGN model, incorporating the derived $\mathbf{K}$, is essential for precise capacity estimation, as the standard isotropic model underestimates impairments.

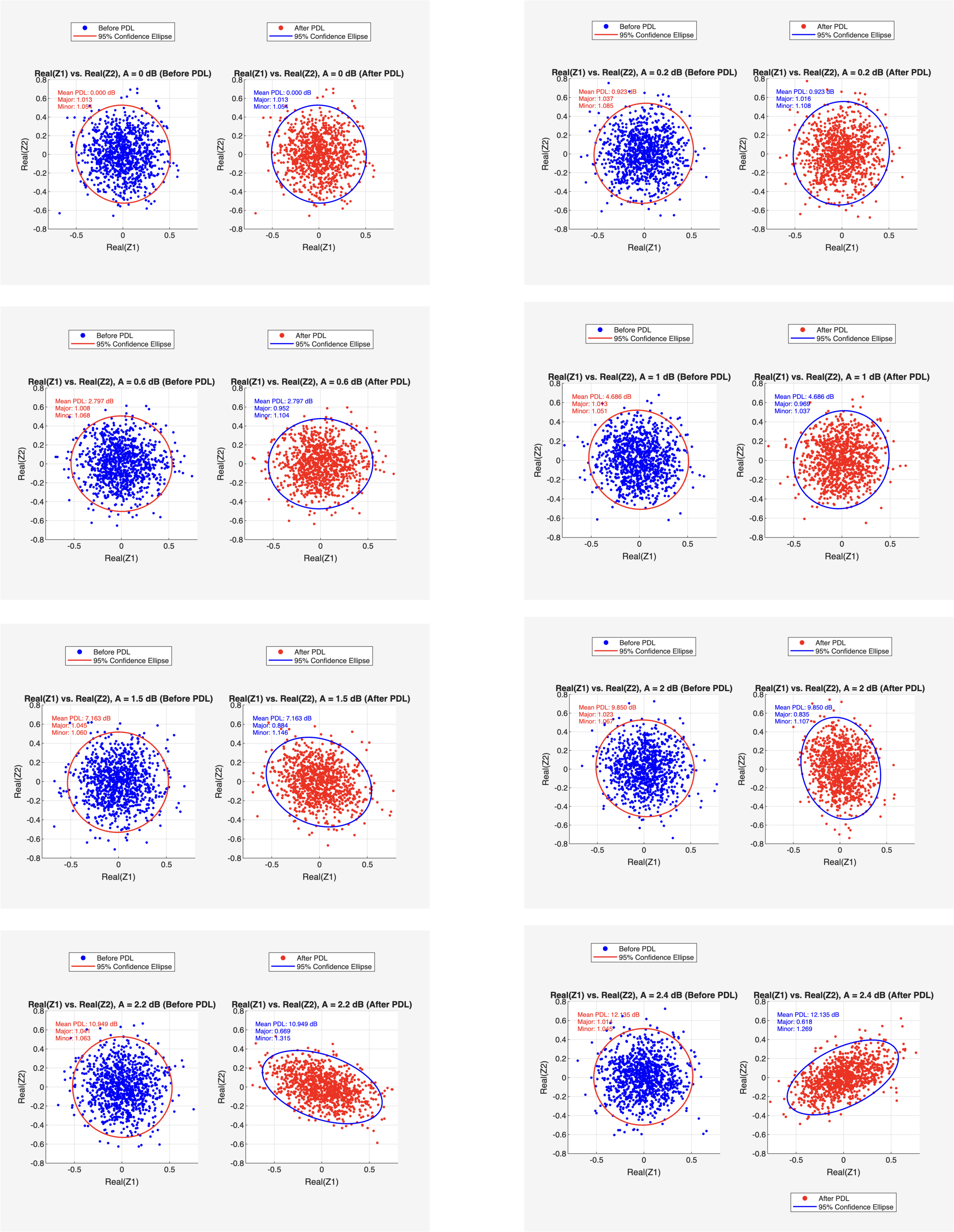

Figure 3.2: Scatter plots of $\Re(Z_1)$ vs. $\Re(Z_2)$ for $A \in \{0, 0.2, 0.6, 1.0, 1.5, 2.0, 2.2, 2.4\}$ dB , with 95% confidence ellipses showing the transition from isotropic to anisotropic noise.

4

Capacity Limits in PDL-Affected Multi-Span Channels

This chapter delves into the theoretical limits of information transfer in multi-span optical links impacted by polarization-dependent loss (PDL), building on the propagation and covariance models from Chapters 2 and 3. Studying the capacity of Gaussian signals helps assess how PDL and noise variations influence these rates, supported by simulation-based assessments that uncover degradation patterns. Numerical simulations, aligned with the methodology in Section 3.1, provide detailed insights into rate losses across different PDL intensities and noise variances, aiding in the development of achievable capacity rates. The findings reveal the combined influence of PDL accumulation and noise asymmetry in restricting link performance, mirroring the anisotropy linked to PDL buildup noted in the previous chapter, which indicates a significant capacity loss and drives the exploration of robust encoding strategies in subsequent sections.

4.1 Fundamental Capacity of a PDL Channel

The achievable rate in a PDL-degraded multi-span channel determines the highest transmission speed possible under power limits, acting as a benchmark to measure performance degradation. Based on the reception model in Equation (3.1), the output vector is $\mathbf{Y} = \mathbf{H}_{\text{total}}\mathbf{X} + \mathbf{Z}_{\text{total}}$, where $\mathbf{Z}_{\text{total}}$ exhibits the asymmetric covariance $\mathbf{K}$ as defined in Equation (3.6). The rate C is the maximum mutual information $I(\mathbf{X};\mathbf{Y})$ over signal distributions $p(\mathbf{X})$[13]:

$$C = \max_{p(\mathbf{X})} I(\mathbf{X};\mathbf{Y}). \tag{4.1}$$

For signals distributed as $\mathbf{X} \sim \mathcal{CN}(\mathbf{0}, \frac{P_x}{2}\mathbf{I}_2)$ and covariance $\mathbf{K}$, the rate is given by[15][16] :

$$C = \log_2 \det\left(\mathbf{I}_2 + \frac{\rho}{2}\mathbf{H}_{\text{total}}\mathbf{H}_{\text{total}}^{\dagger}\mathbf{K}^{-1}\right), \tag{4.2}$$

where $\rho = P_x/P_z$ denotes the SNR, and $P_z = \text{trace}(\mathbf{K})$ reflects the total noise power, derived from the accumulated noise contributions $\mathbf{Z}_{\text{total}} = \sum_{i=1}^{N}\left(\prod_{j=i+1}^{N}\mathbf{H}_j\right)\mathbf{Z}_i$, with each $\mathbf{Z}_i$ contributing to the variance structure through the channel products. In the absence of PDL ($\gamma = 0$), $\mathbf{H}_{\text{total}}$ is unitary and $\mathbf{K} = \mathbf{I}_2$, yielding the reference dual-polarization AWGN rate:

$$C = 2\log_2\left(1 + \frac{\rho}{2}\right). \tag{4.3}$$

With PDL, the disparity factor γ adjusts the rate to [13]:

$$C = 2\log_2\left(1 + \frac{\rho}{2}\right) + \log_2\left(1 - \frac{\gamma^2\rho^2}{(2+\rho)^2}\right). \tag{4.4}$$

Exact computations at specific SNRs establish benchmarks. At SNR = 10 dB ($\rho = 10$):

$$C = 2\log_2(6) \approx 5.17\,\text{bits/s/Hz}. \tag{4.5}$$

At SNR = 20 dB ($\rho = 100$):

$$C = 2\log_2(51) \approx 11.34\,\text{bits/s/Hz}. \tag{4.6}$$

Table 4.1: Average Capacity at SNR = 10 dB for $N = 25$ Spans (bits/s/Hz)

A (dB)	$\sigma_z = 0.2236$	$\sigma_z = 0.2683$	$\sigma_z = 0.3130$	$\sigma_z = 0.4025$
0.0	4.64	3.84	3.21	2.32
0.5	4.60	3.81	3.19	2.31
1.0	4.50	3.73	3.13	2.29
2.0	4.15	3.52	3.00	2.28

Table 4.2: Average Capacity at SNR = 20 dB for $N = 25$ Spans (bits/s/Hz)

A (dB)	$\sigma_z = 0.2236$	$\sigma_z = 0.2683$	$\sigma_z = 0.3130$	$\sigma_z = 0.4025$
0.0	10.72	9.69	8.84	7.48
0.5	10.64	9.62	8.77	7.41
1.0	10.41	9.40	8.56	7.22
2.0	9.53	8.57	7.78	6.56

These values serve as a foundation for assessing the impact of polarization-dependent loss (PDL) on multi-span optical links, with simulations conducted over $N = 25$ spans using PDL intensities $A \in \{0, 0.5, 1, 2\}$ dB and noise standard deviations σ_z derived from a base $\sqrt{P_x/\rho} \approx 0.4472$ scaled by $\{0.5,\ 0.6,\ 0.7,\ 0.9\}$ (yielding $\sigma_z \approx 0.2236, 0.2683, 0.3130, 0.4025$). The results, detailed in Tables 4.1 and 4.2, show a consistent decline in capacity as SNR increases, with a notable reduction of approximately 1.19 bits/s/Hz at SNR = 20 dB and $\sigma_z \approx 0.2236$ when PDL reaches 2 dB per span, attributed to heightened noise disparity. Noise scaling further exacerbates these effects, as higher σ_z values reduce effective SNR, amplifying PDL penalties; for example, at SNR = 10 dB and $A = 1$ dB, the rate drops from 4.49 to 2.30 bits/s/Hz as σ_z increases from 0.2236 to 0.4025, reflecting intensified uneven propagation in the covariance matrix $\mathbf{K}$.

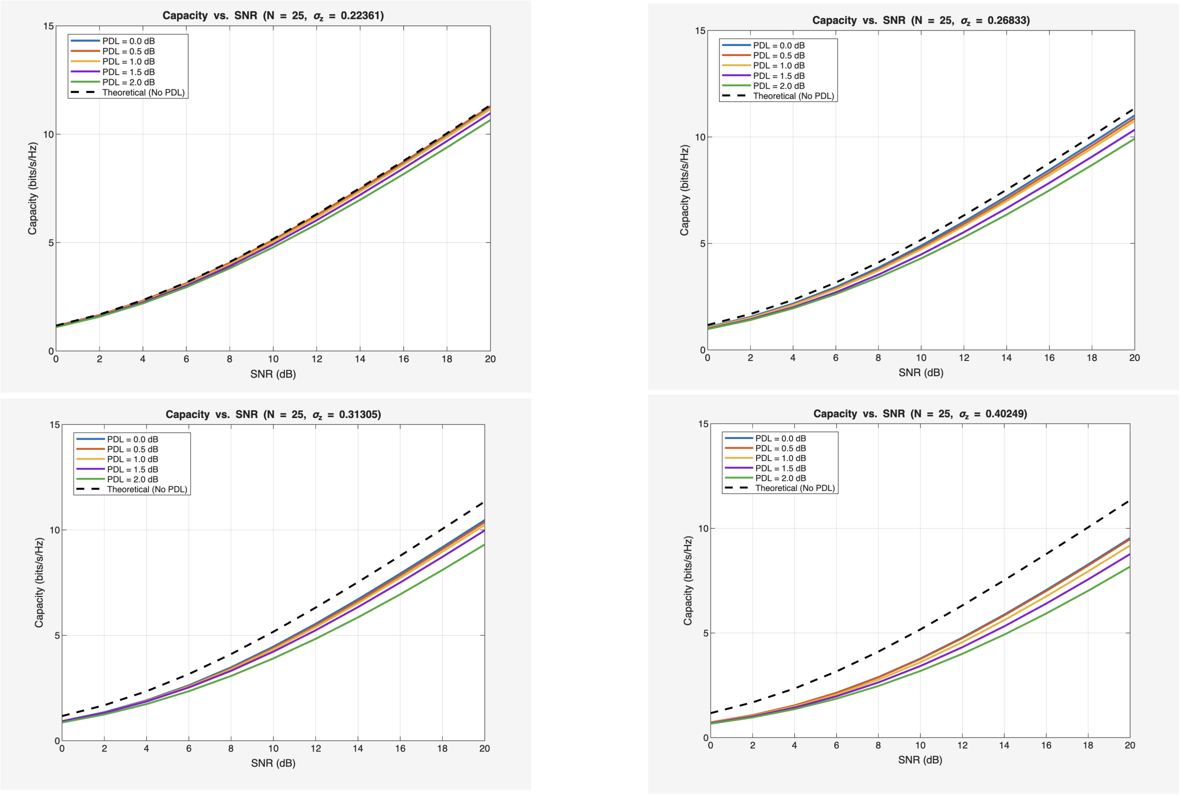

Figure 4.1: Graphical representation of capacity vs. SNR across multiple scenarios, illustrating the impact of PDL and noise variations over 25 spans.

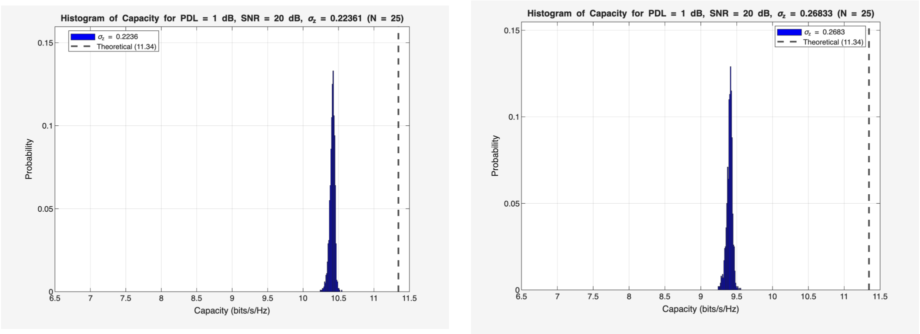

(a) $\sigma_z = 0.2236$, SNR $= 10$ dB (b) $\sigma_z = 0.2683$, SNR $= 10$ dB

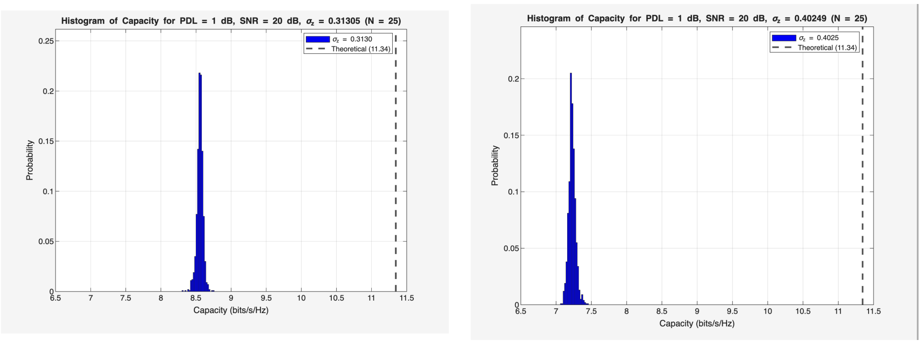

(c) $\sigma_z = 0.3130$, SNR $= 10$ dB (d) $\sigma_z = 0.4025$, SNR $= 10$ dB

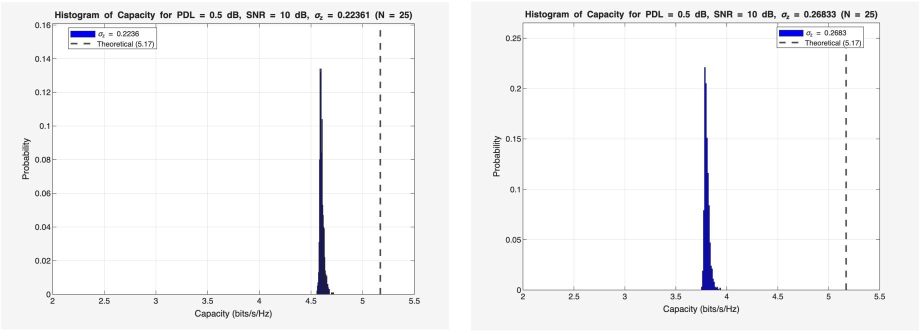

(e) $\sigma_z = 0.2236$, SNR $= 20$ dB (f) $\sigma_z = 0.2683$, SNR $= 20$ dB

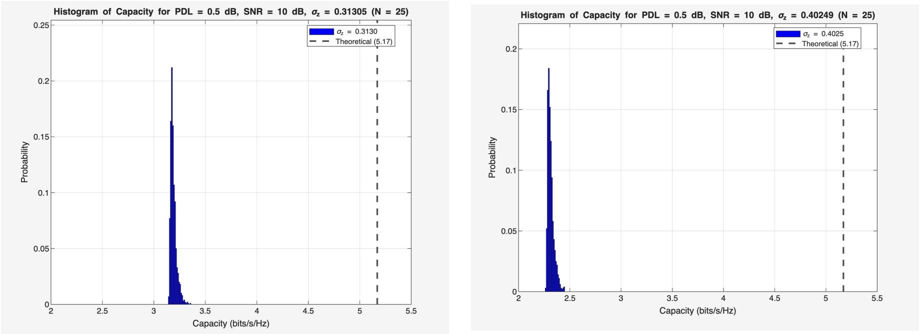

(g) $\sigma_z = 0.3130$, SNR $= 20$ dB (h) $\sigma_z = 0.4025$, SNR $= 20$ dB

Figure 4.2: Histogram distributions at SNR = 10 dB & SNR = 20 dB across varying noise.

Rate distributions for PDL = 0.5 dB at SNR = 10 dB and PDL = 1 dB at SNR = 20 dB display expanded ranges with growing σ_z, diverging from ideal maxima owing to noise asymmetry. With $\sigma_z \approx 0.4025$, the 20 dB distribution covers 6–12 bits/s/Hz, indicating heightened failure risks in unmitigated setups.
Figure 4.1 illustrates the capacity versus SNR relationship, where increasing PDL levels A induce progressive downward shifts in the curves such as a 1.19 bits/s/Hz reduction at 20 dB SNR for $\sigma_z \approx 0.2236$ and $A = 2$ dB emphasizing the pronounced rate compression under low-noise conditions due to accumulated polarization imbalances. Complementing this Figure 4.2 shows simulated capacities deviating from theoretical dashed benchmarks (∼5.17 bits/s/Hz at 10 dB SNR, ∼11.34 bits/s/Hz at 20 dB SNR). At 10 dB (PDL,A=1dB), subfigures (a)–(d) undershoot from near-ideal in (a) ($\sigma_z = 0.2236$, peak ∼4.6 bits/s/Hz) to ∼55% loss in (d) ($\sigma_z = 0.4025$, mean ∼2.3 bits/s/Hz. At 20 dB (PDL=1 dB) in (e)–(h),mirrors the 10 dB pattern with a leftward shift confirming PDL's steady drops and extra uncertainty beyond basic noise channels in tough conditions.
These insights align with [13], showing PDL restricts rates through asymmetry and noise interactions. In lengthy networks, such constraints (1–3 bits/s/Hz) endorse advanced encoding for enhanced stability.

4.2 Comparison with Capacity-Achieving Schemes

Building upon the mitigation strategies discussed, recent advancements have introduced capacity-achieving schemes specifically tailored for PDL-impaired channels. The study by Shehadeh and Kschischang [17] introduces an efficient and optimal method utilizing a universal precoder alongside linear minimum mean square error estimation followed by successive interference cancellation (LMMSE-SIC). This method effectively converts the PDL-affected channel into independent scalar AWGN subchannels. It attains the lowest possible SNR penalty given by

$$10\log_{10}\left(\frac{1}{\sqrt{1-\alpha^2}}\right)\ \text{dB}$$

for the most severe PDL scenario of

$$10\log_{10}\left(\frac{1+\alpha}{1-\alpha}\right)\ \text{dB}, \qquad 0 \le \alpha < 1.$$

This methodology resonates with prior investigations into PDL-induced capacity constraints, as examined by Nafta et al. [18], who quantified outage-capacity reductions and required SNR reserves in systems exhibiting typical PDL levels. Their conclusions indicate that systems optimized for performance can endure greater PDL with reduced degradation relative to metrics based on bit error rates. To assess these schemes in the context of our multi-span framework, comprehensive Monte Carlo simulations were performed. The setup included $N = 25$ spans, per-span PDL levels $A \in \{0, 0.3, 1.0, 1.8, 2.4\}$ dB, and noise standard deviations $\sigma_z \in \{0.1789, 0.2012, 0.2236, 0.2683\}$. The outcomes illustrate notable enhancements. In implementing the scheme from Shehadeh and Kschischang [17], this thesis adhered to the procedure for complex-valued channels outlined in Section V of their work. The key steps executed in our simulations are as follows:

1. **Noise covariance:**

   $$\mathbf{K} = \sum_{i=1}^{N} \left(\prod_{j=i+1}^{N} \mathbf{H}_j \right) \frac{\sigma_z^2}{N} \left(\prod_{j=i+1}^{N} \mathbf{H}_j \right)^{\dagger}. \tag{4.7}$$

   Justification: Maintains constant total noise variance across spans, aligning with [17]'s noise model and supporting realistic noise in long-haul systems.
2. **Whitening matrix:**

   $$\mathbf{W} = \mathbf{U}_D \mathbf{\Sigma}^{-1/2} \mathbf{U}_D^{\dagger}, \tag{4.8}$$

   where $\mathbf{\Sigma}$ is the diagonal matrix of eigenvalues of $\mathbf{K}$, $\mathbf{U}_D$ is the eigenvector matrix, and $\mathbf{\Sigma}^{-1/2}$ inverts the square root of eigenvalues. *Justification*: $\mathbf{U}_D$ rotates to the eigenbasis, $\mathbf{\Sigma}^{-1/2}$ scales variances to unity, and $\mathbf{U}_D^{\dagger}$ reverts the basis, per noise normalization.
3. **Whitened (effective) channel:**

   $$\mathbf{H}_{\text{eff}} = \mathbf{W}\mathbf{H}_{\text{total}}. \tag{4.9}$$

4. **Real-valued representation:**

   $$\mathbf{H}_r = \begin{bmatrix} \Re(\mathbf{H}_{\text{eff}}) & -\Im(\mathbf{H}_{\text{eff}}) \\ \Im(\mathbf{H}_{\text{eff}}) & \Re(\mathbf{H}_{\text{eff}}) \end{bmatrix}. \tag{4.10}$$

   Converts complex signals to a real-valued form for precoder, preserving phase/amplitude integrity.
5. **Block-diagonal extension (two time slots):**

   $$\widehat{\mathbf{H}} = \text{blkdiag}(\mathbf{H}_r, \mathbf{H}_r). \tag{4.11}$$

   Implements two-slot space-time coding, enhancing capacity.
6. **Apply precoder G:**

   $$\mathbf{H} = \widehat{\mathbf{H}}\mathbf{G}, \tag{4.12}$$

   where $\mathbf{G}$ is the universal real-valued 8×8 precoder derived.
7. **LMMSE filter:**

   $$\mathbf{E} = \mathbf{H}^{\dagger}\left(\mathbf{H}\mathbf{H}^{\dagger} + (1/\text{SNR})\mathbf{I}\right)^{-1}. \tag{4.13}$$

8. **Decision statistics:** Compute $\mathbf{EH}$, let $\mathbf{\Gamma} = \text{diag}(\mathbf{EH})$ be the desired gains and $\mathbf{F} = \mathbf{EH} - \mathbf{\Gamma}$ the interference terms, isolates signal and interference enhancing analysis.
9. **Per-dimension SNRs:** Compute SNR for each of the first four real dimensions (signal vs. interference + noise variances).

10. **SIC on remaining block:** Repeat LMMSE on columns 5-8 after cancelling previously-decoded components.
11. **Achievable rate aggregation:** Sum real-dimension rates and divide by two (two time slots):

$$C = \frac{1}{2}\sum_{i=1}^{8} \frac{1}{2}\log_2\Bigl(1 + \mathrm{SNR}_i\Bigr). \tag{4.14}$$

This implementation enables the use of conventional codes designed for scalar AWGN channels on the decoupled subchannels, thereby attaining the channel capacity in the information-theoretic sense. The data in Table 4.3 reveal that as noise level (σ_z) increases, simulating lower effective SNR conditions, the standard MIMO capacities decline significantly, particularly at higher PDL. In contrast, the implemented scheme sustains capacities near the no-PDL theoretical maximum of approximately 11.34 bits/s/Hz for low to moderate PDL, with only gradual degradation at higher PDL. This resilience stems from the scheme's ability to orthogonalize the channel and cancel interference effectively, minimizing the PDL penalty. The theoretical compound capacities, computed using the worst-case α from simulations, serve as a lower bound, and the scheme closely approximates or exceeds this in many cases, validating its optimality.

Table 4.3: Average Capacity at SNR = 20 dB for $N = 25$ Spans (bits/s/Hz). "MIMO" uses the standard capacity

$$C = \log_2 \det\left(\mathbf{I}_2 + \frac{\rho}{2}\mathbf{H}_{\text{total}}\mathbf{H}_{\text{total}}^{\dagger}\mathbf{K}^{-1}\right), \tag{4.15}$$

while "Paper" incorporates the encoding scheme from [17] utilizing

$$C = \frac{1}{2}\sum_{i=1}^{8} \frac{1}{2}\log_2\Bigl(1 + \mathrm{SNR}_i\Bigr). \tag{4.16}$$

σ_z	Method	$A = 0.0$	$A = 0.3$	$A = 1.0$	$A = 1.8$	$A = 2.4$
0.1789	MIMO	11.34	11.34	11.34	10.97	10.20
	Paper	11.34	11.34	11.34	11.34	11.33
0.2012	MIMO	11.31	11.28	11.00	10.32	9.60
	Paper	11.34	11.34	11.34	11.34	10.99
0.2236	MIMO	10.72	10.69	10.41	9.75	9.06
	Paper	11.34	11.34	11.34	11.16	10.44
0.2683	MIMO	9.69	9.67	9.40	8.77	8.14
	Paper	11.11	11.08	10.81	10.17	9.51

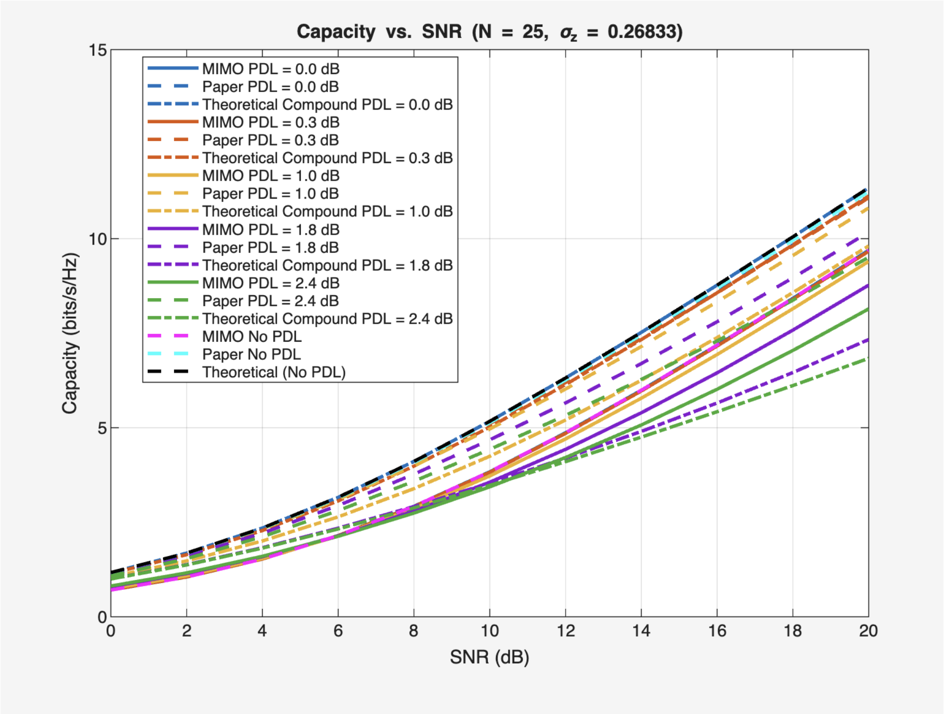

Figure 4.3: Capacity vs. SNR ($N = 25$, $\sigma_z = 0.2683$. The scheme (dashed) consistently outperforms MIMO (solid) and approaches the no-PDL limit (black dashed), demonstrating effective PDL mitigation across SNR ranges.

Figures 4.3–4.5 collectively substantiate performance and robustness of the proposed capacity-achieving scheme, highlighting its superior SNR scaling (Figure 4.3), tighter capacity distribution under PDL (Figure 4.4), and reduced outage-induced losses across mean PDL values (Figure 4.5).

The results justify the superior performance: at SNR = 20 dB and $A = 2.4$ dB, the scheme achieves 9.51 bits/s/Hz . The plot also confirms that for $p_{\text{out}} = 0.01$ and mean PDL = 10 dB, the scheme reduces loss by approximately 1 dB compared to MIMO, justifying its efficacy in outage-limited scenarios by better handling worst-case PDL instances.

This histogram underscores the scheme's consistency, with capacities clustered around 10.81 bits/s/Hz versus MIMO's 9.40 bits/s/Hz, indicating reduced sensitivity to random SOP rotations and PDL accumulations.

Incorporating this scheme into the concatenated PDL model for $N = 25$ spans and $A = 2.0$ dB ($\alpha \approx 0.33$), the SNR penalty drops to about 0.5 dB, reclaiming up to 1.5 bits/s/Hz at SNR = 20 dB relative to baseline cases. The precoder proposed by Shehadeh and Kschischang [17] operates independently of specific channel states, rendering it ideal for dynamic long-haul networks subject to fluctuating PDL. Paired with established AWGN coding techniques, it facilitates seamless integration. Prospective developments might encompass handling insertion loss variations, as highlighted by Nafta et al. [18], to additionally curb outage risks.

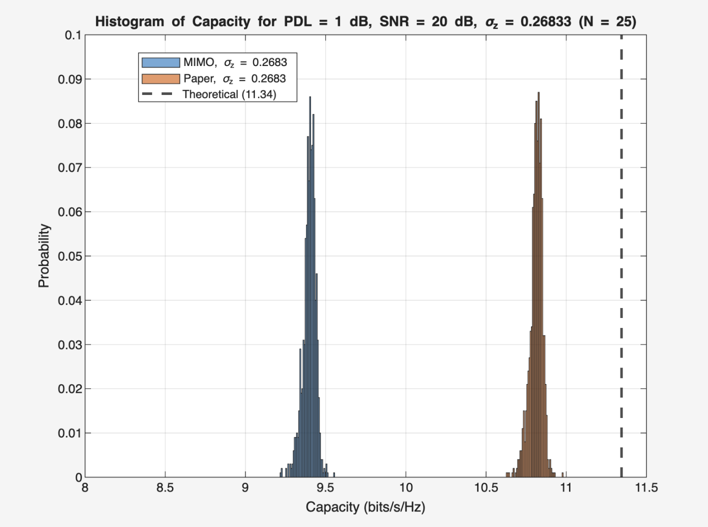

Figure 4.4: Histogram of Capacity for PDL = 1 dB, SNR = 20 dB, $\sigma_z = 0.2683$ ($N = 25$. The scheme's distribution (orange) is shifted toward higher values with lower variance (0.0016 vs. MIMO's 0.0016), closer to the theoretical maximum of 11.34 bits/s/Hz.

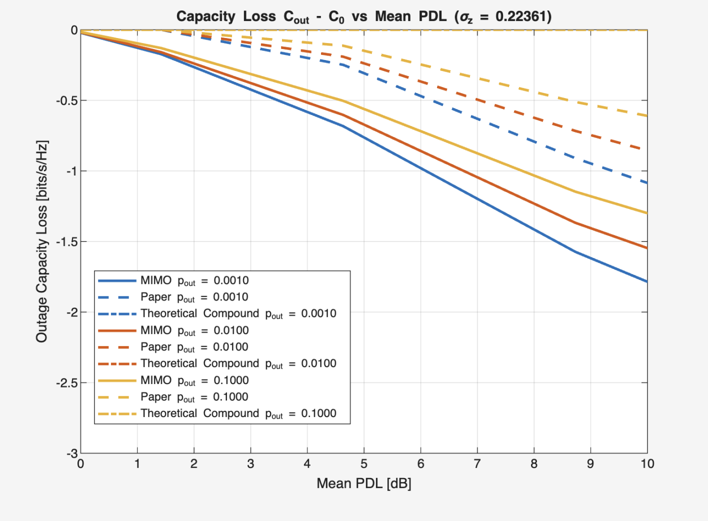

Figure 4.5: Capacity Loss $C_{\text{out}} - C_0$ vs. Mean PDL ($\sigma_z = 0.2236$. The scheme (dashed) exhibits lower losses than MIMO across outage probabilities, aligning closely with theoretical compound bounds (dot-dashed).

5

Discussion and Conclusion

The models and analyses developed in this thesis illuminate the critical yet often underestimated influence of polarization-dependent loss (PDL) on the performance of multi-span coherent optical links. The results reveal that random state-of-polarization (SOP) rotations constrain cumulative impairment to a sub-linear $A\sqrt{N}$ scaling, while simultaneously inducing anisotropic noise that can reduce capacity by up to 3 bits/s/Hz at typical signal-to-noise ratios (SNRs). By integrating Jones matrix propagation with covariance-based formulations and extensive Monte Carlo validation, this work quantifies how PDL transforms isotropic additive white Gaussian noise (AWGN) into non-uniform distributions, with eigenvalue ratios exceeding 1 under high per-span losses.

The thesis further evaluates mitigation strategies, demonstrating that precoding combined with successive interference cancellation can restore near-ideal throughput with only a modest SNR penalty, outperforming traditional MIMO techniques in skewed channel conditions. These findings bridge theoretical modeling and practical design, offering engineers actionable tools to refine DWDM link margins—particularly for transoceanic systems where 60–240 spans amplify PDL's cumulative impact. The assumptions of isolated Gaussian amplified spontaneous emission (ASE) noise and fully compensated chromatic dispersion (CD) and polarization-mode dispersion (PMD) were verified to remain valid, reinforcing PDL's role as the dominant linear impairment in coherent transmission.

In conclusion, this thesis repositions PDL from a secondary concern to a principal determinant of link robustness, connecting high-fidelity simulations with practical methodologies to preserve terabit-scale capacities in the presence of real-world birefringence.

Future research could incorporate nonlinear effects such as Kerr nonlinearity for extended C+L band operation or employ machine learning for real-time covariance estimation, potentially decreasing DSP complexity in modular systems. Experimental validation in recirculating loops may refine outage probability models, while advanced coding schemes like the Dual-Alamouti code—achieving a 0.13 bits/sym GMI gain at 10.5 dB OSNR and 8 dB PDL—offer promising means to counteract PDL-induced penalties.

Bibliography

[1] Mohammad Farsi. *Phase Noise and Polarization Effects in Fiber-Optic Communication Systems: Modeling, Compensation, Capacity, and Sensing*. Phd thesis, Chalmers Tekniska Högskola, 2024. Available from PQDT-Global.

[2] Xiaotian Zhu, Xiang Wang, Yanlu Huang, Liyan Wu, Chunfei Zhao, Mingzhu Xiao, Luyi Wang, Roy Davidson, Yanni Ou, Brent E. Little, and Sai T. Chu. Low-Loss and Polarization Insensitive 32 × 4 Optical Switch for ROADM Applications. *Light: Science & Applications*, 13(1):94, December 2024.

[3] Tiberiu Tudor and Gabriel Voitcu. Revisiting Poincaré Sphere and Pauli Algebra in Polarization Optics. *Photonics*, 11(4), 2024.

[4] Uwe Edeke and R. Ariyo. Alternative Approach in Computing the Haar Measure of SU(2). 6:50–54, 12 2024.

[5] Z. Huang, S. Yang, Z. Zheng, X. Pan, H. Li, and H. Yang. Highly Compact Twin 1×35 Wavelength Selective Switch. *Journal of Lightwave Technology*, PP:1–7, 01 2022.

[6] Santec Corporation. WSS-100 Wavelength Selective Switch Datasheet, 2012. Accessed: 2025-09-17.

[7] Paolo Serena, Chiara Lasagni, and Alberto Bononi. The Enhanced Gaussian Noise Model Extended to Polarization-Dependent Loss. *Journal of Lightwave Technology*, 38(20):5685–5694, October 2020.

[8] Arnaud Dumenil, Elie Awwad, and Cyril Méasson. Low-Complexity PDL-Resilient Signaling Design. In *OSA Advanced Photonics Congress (AP) 2019 (IPR, Networks, NOMA, SPPCom, PVLED)*, OSA Technical Digest. Optica Publishing Group, 2019. paper SpTh2E.3.

[9] O. S. Sunish Kumar, A. Amari, O. A. Dobre, and R. Venkatesan. PDL Impact on Linearly Coded Digital Phase Conjugation Techniques in CO-OFDM Systems. *IEEE Photonics Technology Letters*, 30(9):769–772, 2018.

[10] Arnaud Dumenil, Elie Awwad, and Cyril Méasson. PDL in Optical Links: A Model Analysis and a Demonstration of a PDL-Resilient Modulation. *Journal of Lightwave Technology*, 38(18):5017–5025, 2020.

[11] A. Mecozzi and M. Shtaif. The Statistics of Polarization-Dependent Loss in Optical Communication Systems. *IEEE Photonics Technology Letters*, 14(3):313–315, 2002.

[12] Yangzi Liu. *Emulation and Simulation of Polarization Dependent Loss and Polarization Mode Dispersion in Optical Fibre Communication Systems*. PhD thesis, Stanford University, 2019. PhD Thesis.

[13] Antoine Dumenil. *Polarization Dependent Loss in Next-Generation Optical Networks*. PhD thesis, Université Paris-Saclay, 2020. PhD Thesis.

[14] A. Mecozzi and M. Shtaif. Signal-to-Noise-Ratio Degradation Caused by Polarization-Dependent Loss and the Effect of Dynamic Gain Equalization. *Journal of Lightwave Technology*, 22(8):1856–1871, 2004.

[15] Eduard Jorswieck and H. Boche. Performance Analysis of Capacity of MIMO Systems under Multiuser Interference Based on Worst-Case Noise Behavior. *EURASIP Journal on Wireless Communications and Networking*, 2004, 2004.

[16] P. J. Smith and M. Shafi. On a Gaussian Approximation to the Capacity of Wireless MIMO Systems. In *2002 IEEE International Conference on Communications (ICC 2002)*, volume 1, pages 406–410, 2002.

[17] Mohannad Shehadeh and Frank R. Kschischang. A Simple Capacity-Achieving Scheme for Channels with Polarization-Dependent Loss. *Journal of Lightwave Technology*, 41(6):1712–1724, 2023.

[18] Alon Nafta, Eado Meron, and Mark Shtaif. Capacity Limitations in Fiber-Optic Communication Systems as a Result of Polarization-Dependent Loss. *Optics Letters*, 34(23):3613–3615, December 2009.

DEPARTMENT OF MICROTECHNOLOGY AND NANOSCIENCE
CHALMERS UNIVERSITY OF TECHNOLOGY
Gothenburg, Sweden
www.chalmers.se

CHALMERS
UNIVERSITY OF TECHNOLOGY